INTERNATIONAL ATOMIC ENERGY AGENCY
UNITED NATIONS EDUCATIONAL, SCIENTIFIC AND CULTURAL ORGANIZATION

INTERNATIONAL CENTRE FOR THEORETICAL PHYSICS
34100 TRIESTE (ITALY) - P.O.B. 586 - MIRAMARE - STRADA COSTIERA 11 - TELEPHONE: 2240-1
CABLE: CENTRATOM - TELEX 460392-I

H4.SMR/222 - 23

SECOND AUTUMN WORKSHOP ON

CLOUD PHYSICS AND CLIMATE

(23 November - 18 December 1987)

NUMERICAL WEATHER PREDICTION

S. Tibaldi
Universita degli Studi di Bologna
Bologna, Italy

European Centre

for

Medium Range Weather Forecasts

SEMINAR/WORKSHOP 1982

INTERPRETATION OF NUMERICAL WEATHER PREDICTION PRODUCTS

Seminar : 13 - 17 September

Workshop : 20 - 24 September

Centre Européen pour les Prévisions Météorologiques à Moyen Terme

Europäisches Zentrum für mittelfristige Wettervorhersage

ADIABATIC FORMULATIONS OF THE ECMWF FORECASTING SYSTEM

A. J. Simmons

ECMWF

1. INTRODUCTION

When charged with the task of presenting a summary of the adiabatic formulation of the operational ECMWF forecast model, it is appropriate at this particular point in time to discuss not one formulation, but two. Since August 1979, operational forecasting has been carried out at ECMWF using a second-order accurate finite-difference model with a regular latitude-longitude grid and resolution of 1.875°, a sigma-coordinate and 15-level resolution in the vertical, and a semi-implicit time scheme which allows a time step of 15 minutes in most cases. During this first operational period, one aspect of the Centre's research work has been directed towards the development and testing of alternative adiabatic formulations, and this has led to a new formulation which will shortly replace the current scheme. The new model is based on a spectral technique for the horizontal, a more general terrain-following vertical coordinate than the usual sigma-coordinate, and a semi-implicit time scheme that treats implicitly not only linearized gravity-wave terms, but also the linearized zonal advection of vorticity and moisture. In outlining the two different formulations, an account is thus given both of the model used to produce the results discussed in other contributions to these proceedings, and of the model which will be operational, or very close to becoming operational, by the time these proceedings are published. Mention will be made of differences which may influence the statistical interpretation of the model outputs.

The following section sets out the primitive equations for a moist atmosphere as adopted in both formulations, using a general vertical coordinate. Section 3 then discusses the horizontal discretization, with a summary both of the grid-point and spectral techniques and of the results of the comparisons between these techniques carried out at ECMWF. Aspects of the vertical and temporal discretizations are discussed in Sections 4 and 5. Finally, the incorporation of horizontal diffusion and the treatment of orography are described in Section 6.

2. THE PRIMITIVE EQUATIONS

We consider a general, terrain-following vertical coordinate, a monotonic function of pressure p and dependent on its surface values p_s:

$$\eta = \eta\ (p, p_s) \quad ,$$

where $\eta\ (0, p_s) = 0$ and $\eta\ (p_s, p_s) = 1$. The usual sigma coordinate

(Phillips, 1957) adopted for the adiabatic formulation of ECMWF's original operational model is a special case of this coordinate, with

$$\eta \equiv \sigma = p/p_s .$$

Kasahara (1974) has given the form of the primitive equations for a dry atmosphere using various coordinate systems. The η-coordinate form for a moist atmosphere is set down in this section. Prognostic variables are the horizontal wind components u and v, the temperature T, the specific humidity q and the surface pressure p_s. They are governed by the following equations.

Momentum equation

$$\frac{d\underset{\sim}{v}}{dt} + f\,\underset{\sim}{k} \times \underset{\sim}{v} + \nabla\phi + R_d T_v \nabla \ln p = \underset{\sim}{P}_v + \underset{\sim}{K}_v \qquad (1)$$

Thermodynamic equation

$$\frac{dT}{dt} - \frac{\kappa T_v \omega}{(1+(\delta-1)q)p} = P_T + K_T \qquad (2)$$

Moisture equation

$$\frac{dq}{dt} = P_q + K_q \qquad (3)$$

Continuity equation

$$\frac{\partial}{\partial \eta}\left(\frac{\partial p}{\partial t}\right) + \nabla \cdot \left(\underset{\sim}{v}\frac{\partial p}{\partial \eta}\right) + \frac{\partial}{\partial \eta}\left(\dot{\eta}\frac{\partial p}{\partial \eta}\right) = 0 \qquad (4)$$

Hydrostatic equation

$$\frac{\partial \phi}{\partial \eta} = -\frac{R_d T_v}{p}\frac{\partial p}{\partial \eta} \qquad (5)$$

Here t is time, and $\frac{d}{dt}$ denotes the material derivative, which in η coordinates takes the form

$$\frac{d}{dt} = \frac{\partial}{\partial t} + \underset{\sim}{v} \cdot \nabla + \dot{\eta}\frac{\partial}{\partial \eta} .$$

$\underset{\sim}{v}$ is the horizontal velocity vector, $\underset{\sim}{v} = (u,v,0)$, and ∇ is the two-dimensional gradient operator on a surface of constant η. f is the Coriolis parameter, $\underset{\sim}{k}$ the unit vertical vector, φ the geopotential, R_d the gas constant for dry air, and $\kappa = R_d/C_{pd}$, where C_{pd} is the specific heat of dry air at constant pressure. P_x and K_x denote the rates of change of variable x resulting respectively from parameterized processes (the subject of a separate contribution to these proceedings) and from horizontal diffusion.

An equation for the surface pressure, p_s, is obtained by integrating Eq. (4) from $\eta = 0$ to $\eta = 1$, using the boundary conditions $\dot{\eta} = 0$ at $\eta = 0$ and $\eta = 1$:

$$\frac{\partial p_s}{\partial t} = -\int_0^1 \nabla \cdot \left(\underset{\sim}{v}\frac{\partial p}{\partial \eta}\right) d\eta \qquad (6)$$

while $\dot{\eta}$ and ω are given by

$$\dot{\eta}\frac{\partial p}{\partial \eta} = -\frac{\partial p}{\partial t} - \int_0^\eta \nabla \cdot \left(\underset{\sim}{v}\frac{\partial p}{\partial \eta}\right) d\eta \qquad (7)$$

and

$$\omega = \frac{dp}{dt} = -\int_0^\eta \nabla \cdot \left(\underset{\sim}{v}\frac{\partial p}{\partial \eta}\right) d\eta + \underset{\sim}{v} \cdot \nabla p \qquad (8)$$

where $\frac{\partial p}{\partial t}$ is known in terms of $\frac{\partial p_s}{\partial t}$ from the definition of η.

Moisture effects appear in the momentum, thermodynamic and hydrostatic equations through the virtual temperature, T_v, which is given by

$$T_v = \left(1 + \left(\frac{R_v}{R_d} - 1\right)q\right) T$$

where R_v is the gas constant of water vapour. An additional term $(1+(\delta-1)q)$, where δ is the ratio of the specific heats at constant pressure of water vapour and dry air, is written in the thermodynamic equation. This term was neglected in the adiabatic formulation of the grid-point model, but as it is of the same order as the ratio of temperature and virtual temperature, it is included in the new model. Further detail will be given in the documentation manual of this model.

Equations (1) to (8) may readily be cast into their more familiar form for sigma coordinates by replacing $\partial p/\partial \eta$ by p_s, and $\frac{\partial p}{\partial t}$ by $\sigma\frac{\partial p_s}{\partial t}$. The pressure-gradient term $R_d T_v \nabla \ln p$ becomes equal to $R_d T_v \nabla \ln p_s$ at all levels. In general, the term has the latter value at the surface, and decreases to zero in the case in which coordinate surfaces become surfaces of constant pressure at upper levels. In this case η is independent of p_s for all pressures less than a certain value.

3. THE HORIZONTAL DISCRETIZATIONS

3.1 The grid-point model

A discussion of the adiabatic formulation of the finite-difference model has been given in a series of lectures by Burridge in the 1979 ECMWF Seminar and details will not be repeated here. The model uses a second-order accurate difference scheme based on the staggered grid of variables shown in Fig. 1, the grid known as the C-grid (Arakawa and Lamb, 1977). Choice of this grid was made mainly because of its low computational noise and the ease of implementation of a semi-implicit time scheme. Operationally, a grid interval of 1.875° in latitude and longitude is used, and this resolution is referred to as N48, there being 48 grid intervals between equator and pole. Following the work of Arakawa (1966) and Sadourny (1975) the finite-difference scheme was designed to conserve, among other quantities, the potential enstrophy during vorticity advection by the horizontal flow. Further detail has been given by Burridge and Haseler (1977) and Burridge (1979).

3.2 The spectral model

A more detailed description of the spectral model will be given, although it largely follows the adiabatic formulation described by Baede et al. (1979) in an ECMWF Technical Report. The basic prognostic variables of the model are ζ, D, T, q and $\ln p_s$, where ζ and D are the vorticity and divergence computed on surfaces of constant η:

$$\zeta = \frac{1}{a\cos\theta}\left\{\frac{\partial v}{\partial \lambda} - \frac{\partial}{\partial \theta}(u\cos\theta)\right\}$$

$$D = \frac{1}{a\cos\theta}\left\{\frac{\partial u}{\partial \lambda} + \frac{\partial}{\partial \theta}(v\cos\theta)\right\}$$

where a is the radius of the earth, λ is longitude and θ is latitude. Variables are represented in the horiosntal by truncated series of spherical harmonics:

$$X(\lambda, \mu, \eta, t) = \sum_{m=-M}^{M} \sum_{n=|m|}^{N(m)} X_n^m(\eta, t)\, P_n^m(\mu) e^{im\lambda} \qquad (9)$$

where X is any variable and μ is $\sin\theta$. The $P_n^m(\mu)$ are the Associated Legendre Functions, defined here by

$$P_n^m(\mu) = \sqrt{(2n+1)\frac{(n-m)!}{(n+m)!}}\ \frac{1}{2^{n+1}\,n!}(1-\mu^2)^{m/2}\frac{d^{n+m}}{d\mu^{n+m}}(\mu^2-1)^n\ ,\ m \geq 0, \qquad (10)$$

and

$$P_n^{-m}(\mu) = P_n^m(\mu)$$

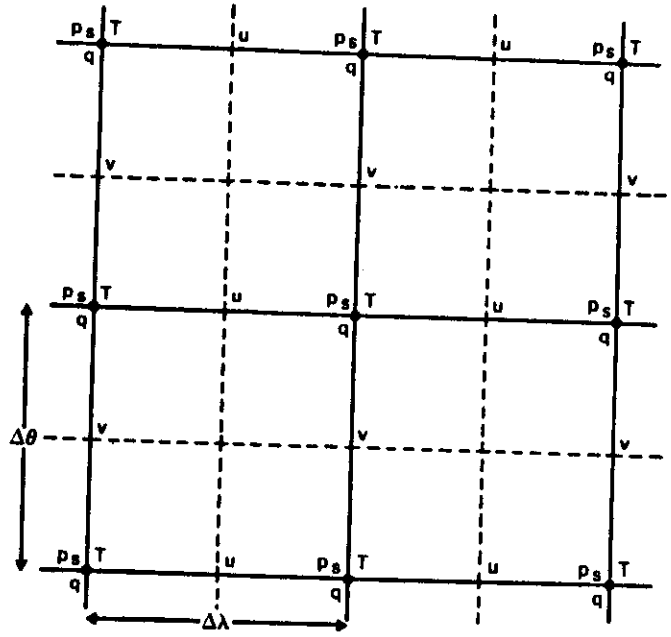

Fig. 1 Horizontal distribution of variables in the grid-point model. Operationally $\Delta\lambda = \Delta\theta = 1.875°$.

and the normalization is such that

$$\frac{1}{2}\int_{-1}^{1} P_n^m(\mu)\, P_s^r(\mu)\, d\mu = \delta_{mr}\,\delta_{ns} \qquad (11)$$

The X_n^m are the complex-valued spectral coefficients of the field X. Since X is real,

$$X_n^{-m} = (X_n^m)^*$$

where $(\ )^*$ denotes the complex conjugate. The model thus deals explicitly only with the X_n^m for $m \geq 0$.

The Fourier coefficients of X, $X_m(\mu,\eta,t)$, are defined by

$$X_m(\mu,\eta,t) = \sum_{n=|m|}^{N(m)} X_n^m(\eta,t)\, P_n^m(\mu) \qquad (12)$$

with

$$X(\lambda,\mu,\eta,t) = \sum_{m=-M}^{M} X_m(\mu,\eta,t)\, e^{im\lambda} \qquad (13)$$

Derivatives are given analytically by

$$\frac{\partial X}{\partial \lambda} = \sum_{m=-M}^{M} im\, X_m\, e^{im\lambda} \qquad (14)$$

and

$$\left(\frac{\partial X}{\partial \mu}\right)_m = \sum_{n=|m|}^{N(m)} X_n^m \frac{dP_n^m}{d\mu} \qquad (15)$$

where the derivative of the Legendre Function is given by the recurrence relation:

$$(1-\mu^2)\frac{dP_n^m}{d\mu} = -n\,\varepsilon_{n+1}^m P_{n+1}^m + (n+1)\,\varepsilon_n^m P_{n-1}^m \qquad (16)$$

with

$$\varepsilon_n^m = \left(\frac{n^2-m^2}{4n^2-1}\right)^{\frac{1}{2}}$$

As in the first ECMWF spectral model (Baede et al., 1979) the model is programmed to allow for a flexible pentagonal truncation, depicted in Fig. 2. This truncation is completely defined by the three parameters J, K and M illustrated in the Figure. The common truncations are special cases of the pentagonal one:

Triangular	M = J = K
Rhomboidal	K = J + M
Trapezoidal	K = J, K > M

The spectral calculation utilizes the transform technique pioneered by Eliasen et al. (1970) and Orszag (1970). It follows that of the early multi-level spectral models described by Bourke (1974) and Hoskins and Simmons (1974), and the ECMWF spectral model reported by Baede et al. (1979), although it differs in its use of an advective rather than a flux form for the temperature and moisture equations. The objective of the calculation is to compute spectral tendencies $\left(\frac{\partial X}{\partial t}\right)_n^m$ for each prognostic variable, from which new values may be computed using the time differencing discussed in Section 5. The orthogonality of the spherical harmonics is such that these spectral tendencies are related to grid-point tendencies by

$$\left(\frac{\partial X}{\partial t}\right)_n^m = \frac{1}{4\pi}\int_{-1}^{1}\int_{0}^{2\pi} \left(\frac{\partial X}{\partial t}\right) P_n^m(\mu)\, e^{-im\lambda}\, d\lambda\, d\mu \qquad (17)$$

An outline of the model's computation of spectral tendencies can now be given. First, a grid of points covering the sphere is defined. Using the basic definition of the spectral expansions (9) and the linear equations relating wind components with vorticity and divergence, values of ζ, D, u,v,T,q and $\ln p_s$ are calculated at the grid points, as also are the required derivatives $\frac{\partial T}{\partial \lambda}$, $\frac{\partial T}{\partial \mu}$, $\frac{\partial q}{\partial \lambda}$, $\frac{\partial q}{\partial \mu}$, $\frac{\partial \ln p_s}{\partial \lambda}$ and $\frac{\partial \ln p_s}{\partial \mu}$ using (12) - (15). The resulting grid-point values are sufficient to calculate the required grid-point contributions to adiabatic tendencies, and also the parameterized tendencies since prognostic surface fields associated with the parameterization are defined and updated on the same grid. The integrands of the prognostic equations of form (17) are thus known at each grid-point, and approximate spectral tendencies are calculated by numerical quadrature. Integration by parts is used to avoid computation of some derivatives:

$$\int_{-1}^{1} \frac{\partial A}{\partial \mu} P_n^m\, d\mu = -\int_{-1}^{1} A \frac{dP_n^m}{d\mu}\, d\mu$$

where $\frac{dP_n^m}{d\mu}$ is known from (16).

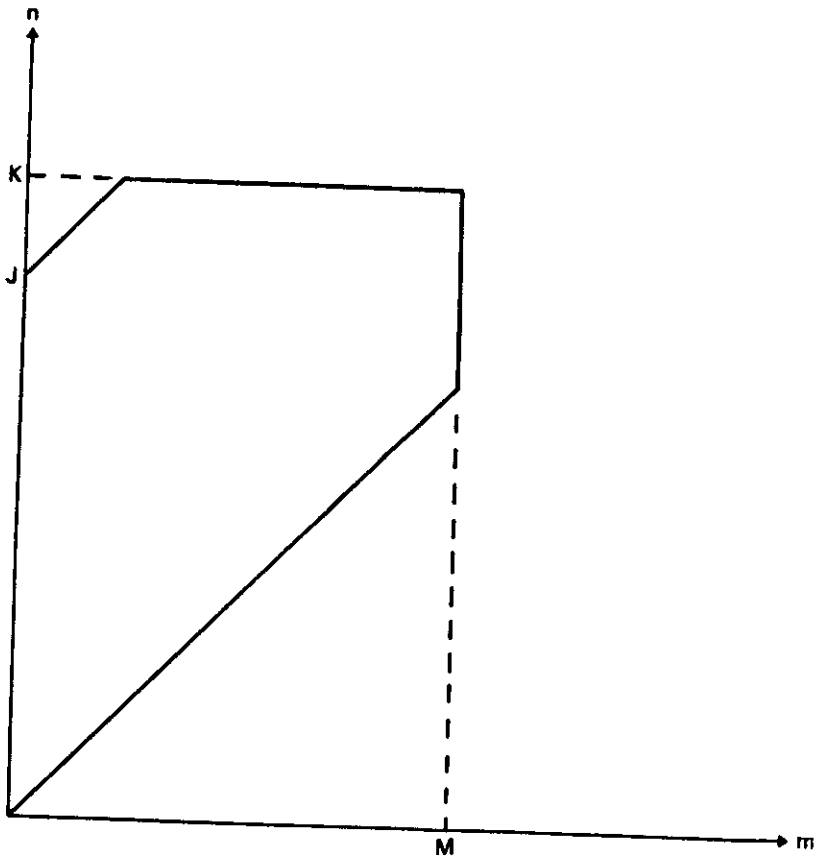

Fig. 2 Pentagonal truncation.

The grid on which the calculations are performed is in fact determined to give an exact (given the spectral truncation of the fields, and within round-off error) contribution to spectral tendencies from quadratic non-linear terms. The integrals with respect to λ involve the product of three trigonometric functions, and as shown by Machenhauer and Rasmussen (1972) they may be evaluated exactly using a regularly-spaced grid of at least 3M+1 points. For the latitudinal integrals, Eliasen et al. (1970) showed that quadratic non-linear terms lead to integrands which are polynomials in μ of a certain order. They may thus be computed exactly using Gaussian quadrature with points located at the (approximately equally-spaced) latitudes which satisfy $P_L^0(\mu) = 0$, for a sufficiently large integer N_G. These latitudes form what are referred to as the "Gaussian latitudes". For triangular truncation, the minimum value of N_G is (3M+1)/2.

It is likely that triangular truncation with M = 63 will be adopted for the first operational version of the spectral model. The associated grid of 192 longitude points and 96 latitude points is a very close equivalent of the regular N48 grid used by the operational grid-point model. Detail in addition to that given here will be found in the documentation manual for the new forecast model.

3.3 The quasi-operational comparison of grid-point and spectral techniques

The primary factor influencing the decision to change operationally to the spectral technique was the better performance of the technique in an extended experiment comparing forecasts performed once per week for a complete year (Girard and Jarraud, 1982). In this experiment, the operational grid-point model forecasts were compared with spectral forecasts using triangular truncation at total wavenumber 63 (T63). The two models used identical parameterization schemes, and required a similar amount of computing resources. Although the models often gave a very similar forecast, some clear differences in overall performance were found. An indication of this is given by Fig. 3, while Fig. 4 presents one example (out of by no means few) of a markedly better local forecast by the spectral model.

A question central to the theme of this particular seminar is to what extent will the change to the spectral model influence statistical forecasts of local weather made using the MOS technique with statistics derived from earlier grid-point forecasts. Insofar as the two models give generally similar large-scale forecasts, with substantial differences found mainly in the medium range in places and cases where the grid-point model is subject to a significant error in its prediction of the synoptic scale, the use of spectral forecasts in conjunction with statistics produced using the grid-point model output should not cause

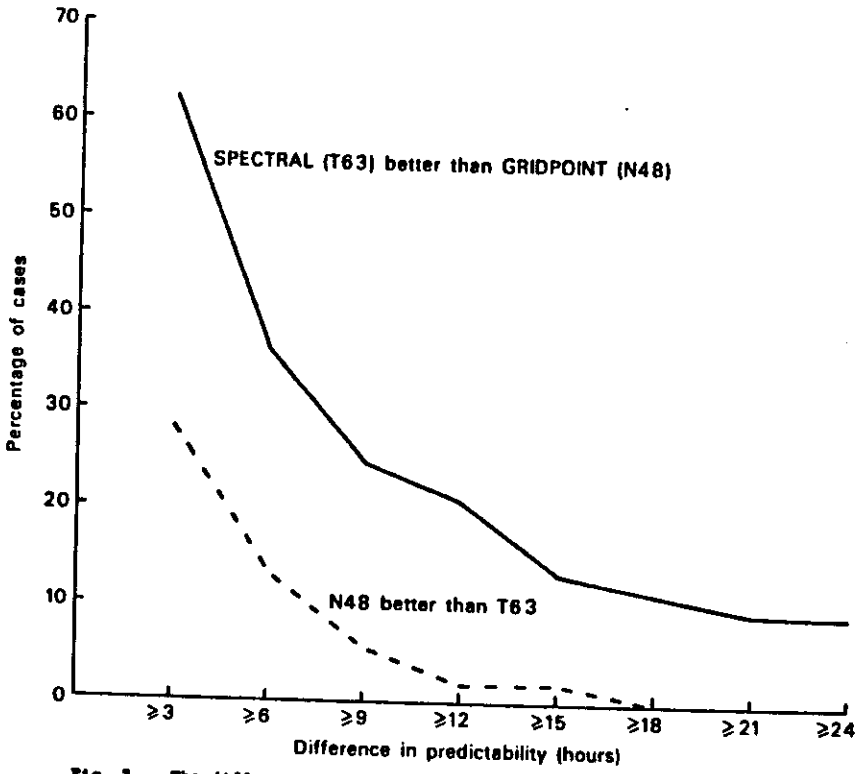

Fig. 3 The difference in predictability (measured by the length of the forecast period for which the anomaly correlation of the 1000 mb height over the extratropical Northern Hemisphere remains above 60%) between spectral (T63) and grid-point (N48) models. Results are expressed in terms of the percentage of cases for which one or other model gave better results.

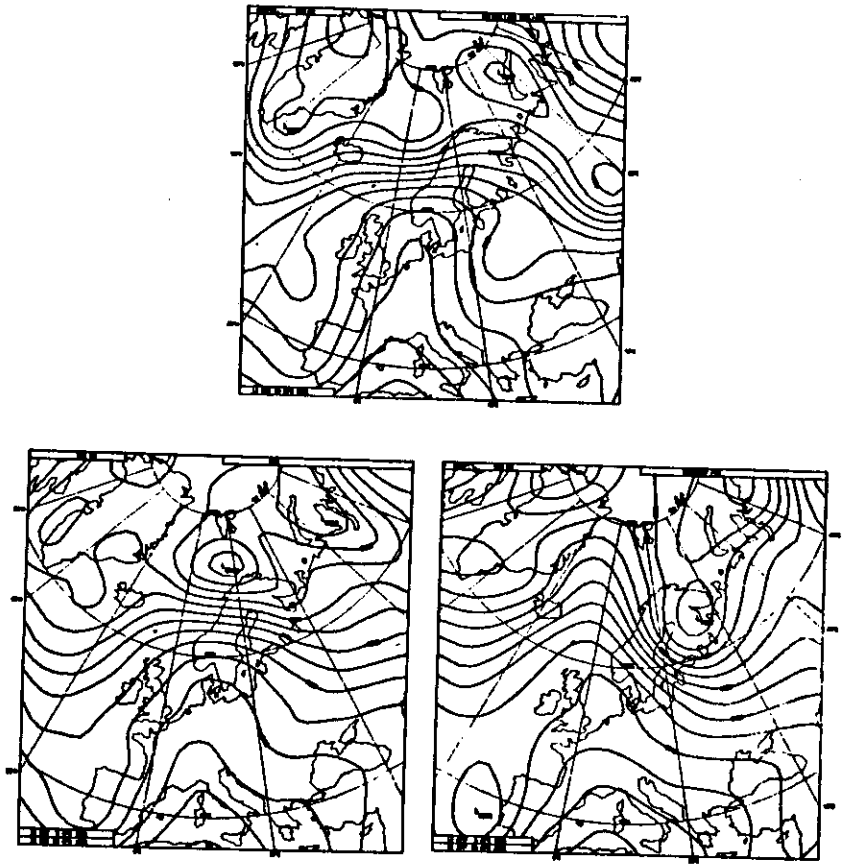

Fig. 4 The analyzed 500 mb height for 10 April, 1981 (upper) and 5-day forecasts for this date by the T63 spectral model (lower left) and the N48 grid-point model (lower right).

particular problems, with the statistical forecasts benefiting from the improved model prediction of the large-scale flow. Two points should, however be borne in mind.

The first concerns some systematic differences in phase speed found between the two models. Statistics presented in Table 1 from the quasi-operational comparison show phase speeds to be generally better represented by the spectral model, at least in the short range (for which an unambiguous identification of analyzed and forecast lows was possible). In view of such differences, use of model predictors at times shifted from the forecast time of interest in order to compensate for systematic phase errors in synoptic-scale systems should evidently be treated with caution.

Table 1 Errors in the displacement (in degrees longitude) of surface lows between day 1 and day 2 of the forecasts for spectral (T63) and grid-point (N48) model forecasts.

Displacement (D)	Cases	Error (Degrees) T63	N48
$D < 5^{o}$	64	+ .6	+1.0
$5^{o} < D < 10^{o}$	39	+ .3	+ .2
$10^{o} < D$	89	-1.8	-2.6
$15^{o} < D$	44	-1.8	-3.3
$20^{o} < D$	16	-2.9	-4.5

The second point concerns the use of model surface and near-surface parameters. If the parameter in question is particularly sensitive to the nature of the model surface (whether it be land or sea, its height, etc.), then caution is again called for, since the different location of grid-points in the new model may give rise to differences in surface and near surface parameters interpolated from neighbouring grid-points in the vicinity of coastlines and steep orography.

4. THE VERTICAL DISCRETIZATION

The vertical variation of the dependent variables is represented by dividing the atmosphere into a number (NLEV) of layers as illustrated in Fig. 5. In general these layers are defined by the pressure of the interfaces between them (the "half-levels"). Prognostic variables are defined at intermediate levels (the "full-levels"). The precise location of these full levels is not required by the adiabatic formulation (apart from the topmost level) since it generally uses only half-level pressures. Full-level pressures need to be specified, however, for the initial analysis of data and for use in the parameterization schemes.

In the operational grid-point model a sigma coordinate is used, with half levels

$$p_{k+\frac{1}{2}} = \sigma_{k+\frac{1}{2}} p_s \quad , k = 0,1,2,\ldots NLEV, \tag{18}$$

and full levels

$$p_k = \sigma_k p_s \tag{19}$$

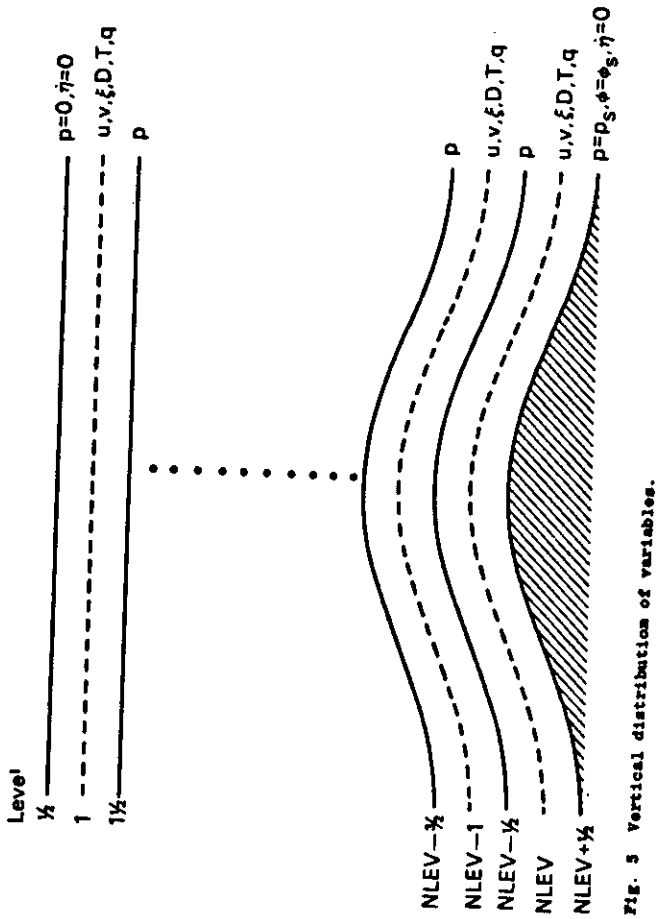

Fig. 5 Vertical distribution of variables.

15 levels are used, and the sigma values are given for both half and full levels by

$$\sigma_k = .75\, s_k + 1.75\, s_k^3 - 1.5\, s_k^4 \qquad (20)$$

where $s_k = (k-\frac{1}{2})/15$. Full-level pressures are given in the left-hand column of Table 2.

In the new model, a more general specification of half-level pressures is adopted:

$$p_{k+\frac{1}{2}} = A_{k+\frac{1}{2}} + B_{k+\frac{1}{2}}\, p_s \qquad (21)$$

with full-level values given by

$$p_k = \tfrac{1}{2}\,(p_{k-\frac{1}{2}} + p_{k+\frac{1}{2}}) \qquad (22)$$

Necessary values are

$$A_{\frac{1}{2}} = B_{\frac{1}{2}} = A_{NLEV+\frac{1}{2}} = 0 \quad , \quad B_{NLEV+\frac{1}{2}} = 1$$

The sigma-coordinate form is reproduced by setting all the $A_{k+\frac{1}{2}}$ to zero, while zero upper-level values of $B_{k+\frac{1}{2}}$ imply that the vertical coordinate is locally a pressure coordinate. Advantages of a hybrid coordinate which transforms smoothly from a sigma coordinate at low levels to a pressure coordinate at upper levels have been discussed by Simmons and Burridge (1981), and Sirmonn and Strüfing (1981).

Final details of the operational implementation of the new coordinate remain to be finalized, but a radical change in the number or location of levels is unlikely. In particular, the stratospheric resolution over the sea will be essentially unchanged in the first instance, although the topmost one or two levels will be constant-pressure levels if final testing proves satisfactory. Once the system is established operationally, testing of alternative resolutions coincident with the resolution of the stratospheric pressure-level analysis, a possibility which is a potential advantage of the new formulation, will take place.

A minor change in resolution may occur, however, and a possible distribution of 16 full-level pressures is given in Table 2. Above the planetary boundary layer, levels differ little from those of the operational grid-point model, the extra level being used to give a less rapid variation in vertical resolution close to the ground.

Table 2 Full-level pressures (mb) for the original operational model and possible alternatives for the new operational model. Values are for a surface pressure of 1000 mb.

LEVEL	PRESSURE (mb)	
	Original Operational Model	New Operational Model
1	25	25
2	77	75
3	132	128
4	193	185
5	260	250
6	334	324
7	415	406
8	500	496
9	589	589
10	678	681
11	765	769
12	845	846
13	914	909
14	967	955
15	996	982
16		996

The motivation behind the proposed change is to give an unambiguous treatment of the lowest model level. The form of the function (20) defining both full and half-level sigma values is such that the lowest full-level is defined to have a value of sigma approximately equal to

$$1 - \Delta\sigma_{15}/4$$

where $\Delta\sigma_{15}$ is the difference in σ between the ground ($\sigma_{15\frac{1}{2}} = 1$) and the next level ($\sigma_{14\frac{1}{2}}$). In particular, this value is used to define the height of the lowest full level in the boundary layer parameterization. Conversely, the vertical finite-difference scheme for the adiabatic model effectively assumes the lowest level to be at

$$\sigma = 1 - \Delta\sigma_{15}/2$$

There is thus an ambiguity in the treatment of the lowest model level, and this can only be removed by adding an additional level if the resolution is constrained to be essentially unaltered in the free atmosphere and to give an unchanged height of the lowest model level in the boundary-layer scheme. The impact of this possible change on the large-scale forecast is unlikely to be large, although it remains to be seen whether near-surface model fields exhibit an improved behaviour.

The vertical finite-difference scheme for the first operational model has also been described in detail in an earlier seminar (Burridge, 1979), and details will not be repeated here. The representation of the $\frac{\kappa T_v \omega}{p}$ term in (2) is such that the change in potential energy associated with it balances the change in kinetic energy due to the term $\underline{v}.(\nabla\phi + R_d T_v \nabla \ln p)$ that arises in the kinetic energy equation derived from (1). In addition, energy conservation is preserved by the formulation of the vertical advection terms: the representation of $\dot{\eta}\frac{\partial X}{\partial \eta}$ for any variable X is such that

$$\sum_{k=1}^{NLEV} X_k \Delta p_k \quad \text{and} \quad \sum_{k=1}^{NLEV} X_k^2 \Delta p_k$$

are not changed due to finite-difference errors in the treatment of this term. Here X_k denotes the value of X at level k, and $\Delta p_k = p_{k+\frac{1}{2}} - p_{k-\frac{1}{2}}$.

The vertical finite-difference scheme used in the new formulation (21) is a straightforward extension of the sigma-coordinate scheme, and has been discussed by Simmons and Burridge (1981) and Simmons and Strüfing (1981). The only point of difference lies in the choice of a representation of the $\nabla\phi + R_d T_v \nabla \ln p$ term in (1) which ensures no spurious generation or dissipation of angular momentum due to vertical truncation error. The impact of this change on sigma

coordinate forecasts has been found to be extremely small, but idealized calculations of pressure-gradient error over sloping ground for a temperature field dependent only on pressure have indicated that this error is reduced for a hybrid coordinate by choosing the angular-momentum conserving scheme rather than simpler alternative finite-difference approximations (Simmons and Strüfing, 1981).

Simmons and Strüfing (loc. cit.) have also reported on forecast tests using the new vertical scheme. Overall, new and old schemes gave a very similar performance, although the differences that were found generally favoured the new system. The new scheme was not tested in data assimilations, where a further small benefit might be anticipated.

5. TIME SCHEMES

Burridge (1979) has also discussed the semi-implicit time-stepping scheme adtoped for the operational grid-point model, and only the barest outline of the scheme, which derives from the work of Robert et al. (1972), will be given here. If X is a model variable satisfying the equation

$$\frac{\partial X}{\partial t} = \dot{X}$$

the time-scheme for adiabatic terms is formally written

$$X(t+\Delta t) = \bar{X}(t-\Delta t) + 2\Delta t \{\dot{X}(t) + \tfrac{1}{2}[\dot{X}_g(t+\Delta t) + \dot{X}_g(t-\Delta t) - 2\dot{X}_g(t)]\} \qquad (23)$$

with

$$\bar{X}(t) = X(t) + \alpha[X(t+\Delta t) + \bar{X}(t-\Delta t) - 2X(t)] \qquad (24)$$

In Eq. (23), X_g represents that component of X associated with linear gravity wave motion about a resting basic state with temperature $T_r(\sigma)$, and the implicit treatment of X_g terms ensures that the time-step criterion is not determined by the rapid ($\approx 300\ ms^{-1}$) phase speed of the model's fastest gravity wave. Eq. (24) describes the time filter analyzed by Asselin (1972), which acts to inhibit the growth of the spurious computational mode associated with the leap-frog scheme.

Operationally, an isothermal reference temperature, with $T_r = 300$ K, is used, a choice governed by the computational stability properties of the semi-implicit technique (Simmons et al., 1978). The value of the time-filtering parameter α is 0.05. A timestep Δt of 15 minutes is generally used with the model, although very strong winds in the polar-night jet of the Southern Hemisphere stratosphere have necessitated a reduction to 12 minutes in September both in 1981 and in 1982.

The extension of the semi-implicit method to the hybrid vertical coordinate discussed in the preceding section has been described by Simmons and Burridge (1981) and Simmons and Strüfing (1981), who also discuss how additional care must be taken in the choice of reference state for this coordinate. Also in the context of the new operational model, an extension of the semi-implicit technique will be introduced. Following results obtained by Robert (1981), who showed that in a semi-implicit shallow-water equation model the time-step limit was determined by the explicit treatment of the vorticity equation, an implicit treatment of the linearized zonal advection of vorticity and moisture will be included. The time-step to be used remains a matter for experimentation.

6. HORIZONTAL DIFFUSION AND THE PRESCRIPTION OF OROGRAPHY

Ideally, the horizontal diffusion that is represented by the K_x terms on the right-hand sides of Eqs. (1)-(3) would be regarded as representing the influence of unresolved scales of motion on the explicitly forecast scales and treated with a physically based parameterization scheme. In practice, since the smallest scales in a model are inevitably subject to numerical misrepresentation, it is common to chose empirically a computationally convenient form for horizontal diffusion and adjust it to ensure that fields of interest do not become excessively noisy. Such an approach has been adopted at ECMWF, and some results may be found in Technical Memoranda by Jarraud and Cubasch (1979) and Strüfing (1982).

The diffusion scheme used operationally since March 1980 may be written in the form

$$K_x = k D^4 X + C_x \qquad (25)$$

The operator D^4 is given for the grid-point model by

$$D^4 = \frac{1}{a^4}\left(\frac{1}{\cos^4\theta}\delta_\lambda^4 + \delta_\theta^4\right) \qquad (26)$$

where

$$\delta_x X = \frac{1}{\Delta x} \{X(x + \Delta x/2) - X(x - \Delta x/2)\}$$

and the diffusion coefficient k has the value 4.5×10^{15} $m^4 s^{-1}$ in the operational forecasts, a value twice as large being used in data assimilation cycles. The operator δ_θ^4 is computed on values at time-step t-Δt, while δ_λ^4 is applied on the value for t+Δt using Fourier analysis and synthesis. This implicit treatment enables the model to be integrated without any additional spatial filtering to counteract the influence of the convergence of meridians on the time-step criterion.

The term C_x in (25) represents a correction connected with the forecasting of precipitation in mountainous areas. After the introduction of a new steeper orography in April 1981, the uncorrected scheme was found to elad to highly unrealistic precipitation patterns and amounts near mountains. Since the diffusion scheme mixed temperatures on model sigma surfaces, it tended to warm spuriously the mountain tops, and this leads to spurious convection and precipitation.

The ideal way of preventing this happening would be to apply the diffusion on the quasi-horizontal surfaces of constant pressure, but this would not be straightforward to implement, and would be computationally expensive. As a compromise, the following correction operators on temperature and humidity were introduced operationally:

$$C_T = \left(\frac{\partial T}{\partial \ln \sigma}\right) D^4 \ln p_s$$

$$C_q = \frac{q}{q_s} \frac{\partial}{\partial \ln \sigma} q_s \; D^4 \ln p_s$$

where q_s denotes the saturation specific humidity. This appears to have largely solved the problem, although it is evident that forecast precipitation must be treated with particular caution in mountainous areas.

Horizontal diffusion in the spectral model also is in the form (25), but with D^4 now representing the ∇^4 operator. Thus in the absence of a correction,

$$K_x = - k \nabla^4 x$$

and

$$(K_x)_n^m = - \frac{k}{a^4} n^2 (n+1)^2 x_n^m$$

It is also applied at time-step t+Δt. The diffusion coefficient used for most past experimentation is smaller than that used in the grid-point model: $k = 7 \times 10^{14}$ $m^4 s^{-1}$. This lessens the liklihood of spurious precipitation near mountains, and this problem may also be lessened by use of the hybrid vertical coordinate (Simmons and Strüfing, 1981). If necessary, a correction of the type used in the grid-point model may be applied operationally, but datails remain to be finalized.

A further remark about the prescription of the orography is also appropriate. A study by Wallace et al. (1983) has indicated that a significant part of the systematic error in the operational forecasts of the extratropical height field may be due to inadequate orographic forcing of the large-scale flow, and has shown use of a higher "envelope" orography to result in significant improvements in the medium-range forecasts for a mid-winter period. It thus appears likely that another change in the prescription of orography will take place when further research has been completed. This should be noted when using model output statistics for mountainous areas.

REFERENCES

Arakawa, A. 1966 Computational design for long-term numerical integration of the equations of fluid motion: two-dimensional incompressible flow. Part I. J. Comp. Phys., 1, 119-143.

Arakawa, A. and V.R. Lamb 1977 Computational design of the basic dynamical processes of the UCLA general circulation model. Methods in Computational Physics, 17, J. Chang, Ed., Academic Press, 337 pp.

Asselin, R. 1972 Frequency filter for time integrations. Mon. Wea. Rev., 100, 487-490.

Baede, A.P.M., M. Jarraud and U. Cubasch 1979 Adiabatic formulation and organization of ECMWF's spectral model. ECMWF Technical Report No. 15, 40 pp.

Bourke, W. 1974 A multi-level spectral model: I Formulation and hemispheric integrations. Mon. Wea. Rev., 102, 688-701.

Burridge, D.M. 1979 Some aspects of large scale numerical modelling of the atmosphere. Proceedings of ECMWF Seminar on Dynamical Meteorology and Numerical Weather Prediction, Vol. 2, 1-78.

Burridge, D.M. and J. Haseler 1977 A model for medium range weather forecasting - Adiabatic formulation. ECMWF Technical Report No. 4, 46 pp.

Eliasen, E., B. Machenhauer and E. Rasmussen 1970 On a numerical method for integration of the hydrodynamical equations with a spectral representation of the horizontal fields. Inst. of Theor. Met., Univ. of Copenhagen, Report No. 2.

Girard, C. and M. Jarraud 1982 Short and medium range forecast differences between a spectral and a grid-point model. An extensive quasi-operational comparison. ECMWF Technical Report No. 32. 178 pp.

Hoskins, B.J. and Simmons, A.J. 1975 A multi-layer spectral model and the semi-implicit method. Quart. J.R. Met. Soc., 101, 637-655.

Jarraud, M. and U. Cubasch 1979 Horizontal diffusion experiments with the ECMWF spectral model. ECMWF Technical Memorandum No. 8, 17 pp.

Kasahara, A. 1974 Various vertical coordinate systems used for numerical weather prediction. Mon. Wea. Rev., 102, 509-522.

Machenhauer, B. and E. Rasmussen 1972 On the integration of the spectral hydrodynamical equations by a transform method. Inst. of Theor. Met., Univ. of Copenhagen, Report No. 4.

Orszag, S.A. 1970 Transform method for calculation of vector coupled sums: application to the spectral form of the vorticity equation. J. Atmos. Sci., 27, 890-895.

Phillips, N.A. 1957 A coordinate system having some special advantages for numerical forecasting. J. Met., 14, 184-185.

Robert, A.J. 1981 A stable numerical integration scheme for the primitive meteorological equations. Atmos. Ocean, 19, 35-46.

Robert, A.J. 1982 A semi-Lagrangian and semi-implicit numerical integration scheme for the primitive meteorological equations. J. Met. Soc. Japan, 60, 319-325.

Robert, A.J., J. Henderson and C. Turnbull 1972 An implicit time integration scheme for baroclinic models of the atmosphere. Mon. Wea. Rev., 100, 329-335.

Sadourny, R. 1975 The dynamics of finite difference models of the shallow-water equations. J. Atmos. Sci., 32, 680-689.

Simmons, A.J. and D.M. Burridge 1981 An energy and angular-momentum conserving vertical finite-difference scheme and hybrid vertical coordinates. Mon. Wea. Rev., 109, pp. 758-766.

Simmons, A.J. and R. Strüfing 1981 An energy and angular-momentum conserving finite-difference scheme, hybrid coordinates and medium-range weather prediction. ECMWF Technical Report No. 28, 68 pp.

Simmons, A.J., B.J. Hoskins and D.M. Burridge 1978 Stability of the semi-implicit time scheme. Mon. Wea. Rev., 106, 405-412.

Strüfing, R. 1982 Some comparisons between linear and non-linear horizontal diffusion schemes for the ECMWF grid-point model. ECMWF Technical Memorandum No. 60, 42 pp.

Wallace, J.M., S. Tibaldi and A.J. Simmons 1983 Reduction of systematic forecast errors in the ECMWF model through the introduction of an envelope orography. Submitted to Quart. J. Roy. Met. Soc.

PARAMETERIZATION OF SUB-GRID SCALE PROCESSES.

J.F.Louis

ECMWF

1. INTRODUCTION

The role of the parameterization in the forecast model is to take into account the physical forcings which make the equations not purely adiabatic. This includes the exchange of momentum, heat and moisture at the earth's surface, the horizontal and vertical eddy fluxes of the same quantities, the effect of precipitation and radiative exchanges.

I shall not expand on the horizontal diffusion. Although it should represent the effect of the sub-grid scale horizontal fluxes that arise from the discretization of the model, it is in fact used mainly as a mathematical device to control numerical noise in the integration. In the operational model it is done with a linear, fourth order scheme, which is implicit in the east-west direction.

My purpose, in this paper, is not to give a detailed mathematical description of all parts of the parameterization schemes of the ECMWF model. Such a description can be found in the Forecast Model Documentation Manual and in other published papers (Louis,1979, Geleyn and Hollingsworth,1979). I shall try, instead, to give the reader an idea of the general principles on which our methods are based, with only enough details to understand the forecast products which are derived from the sub-grid scale parameterization, (namely the near surface temperature and winds, the precipitation and the forecast cloudiness).

2. BOUNDARY LAYER FLUXES

Under this heading I include the surface exchanges as well as the eddy fluxes in the atmosphere. Even though those fluxes are most important in the boundary layer, they are computed throughout the model atmosphere since they can provide a fair amount of dissipation and mixing in region of large vertical shear such as near the jet stream. Results from the surface fluxes computations are also used to determine the two-metre temperature and the ten-metre wind which are among the experimental products of the Centre.

The distribution of levels in the forecast model is such that we can resolve some structure in the boundary layer. As can be seen on figure 1, we have four levels in the lowest 1500 m of the atmosphere, and the lowest level is at about 30 m. Note that the heights shown on the figure are approximate heights above the ground, computed for a standard atmosphere.

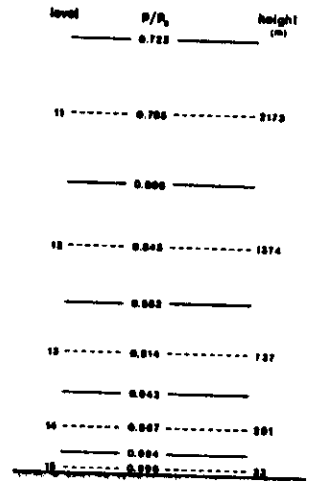

Fig. 1 Vertical distribution of the model levels near the ground

We use the winds and temperature of the lowest level, as well as the ground surface temperature, to compute the fluxes at the surface, according to a drag law. It is well known, however, that surface fluxes are not only dependent on the wind shear at the surface, as in the simplest drag law, but are a strong function of stability. We have used the Monin-Obukhov similarity theory to determine the behaviour of the surface fluxes in terms of the stability.

This theory assumes that, near the ground, the local vertical gradients of potential temperature and wind depend only on the height, the surface fluxes of heat and momentum, and the expansion coefficient of the air. Then, by integrating these flux-gradient relationships between the roughness length z_o and the lowest model level h, it can be shown that the surface fluxes are related to the wind at the lowest model level ∇_h and the potential temperature difference $\Delta\theta_h$ in the lowest layer through universal functions of h/z_o and the Richardson number R_i given by

$$Ri = g\, h\, \Delta\theta_h \,/\theta \left|\nabla_h\right|^2 \qquad (1)$$

Hence the expressions for the surface fluxes can be written

$$P_M = [\, k \,/\, \ln(h/z_o)\,]^2 \cdot F(h/z_o, Ri)\, \left|\nabla_h\right| \nabla_h$$

$$P_H = [\, k \,/\, \ln(h/z_o)\,]^2 \cdot G(h/z_o, Ri)\, \left|\nabla_h\right| \Delta\theta_h \qquad (2)$$

in a way which shows the logarithmic profiles in neutral conditions (i.e. when F=G=1). The constant k is von Karman's constant.

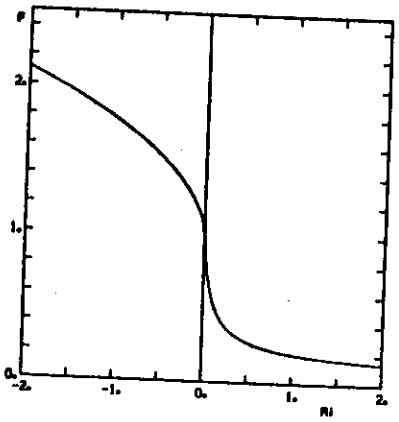

Fig. 2 Variation of the normalized drag coefficient in terms of the Richardson number, for $h/z_o = 50$.

The analytical form of the functions F and G is not uniquely defined. In the course of two years of operational forecasts, we have in fact changed them twice, on the basis of observations and performance of the model. The variation of F with the stability parameter Ri in the current operational model is shown on figure 2 for h/z_o=50. This curve represents the ratio between the drag coefficient under varying stability to the one for a neutral atmosphere.

Above the surface layer we have extended the similarity arguments by assuming that, if the model layers are thin enough, the wind and temperature gradients should depend only on the fluxes through the layer, the expansion coefficient, and a mixing length which is a function of height only. The diffusion coefficients are then related to the Richardson number of the layer through formulae very similar to (2).

It should be noted that the effect of moisture on stability must be taken into account since water vapour is lighter than dry air. This is done by using the virtual potential temperature in the definition of the Richardson number.

The two-metre temperature and the ten-metre wind which are disseminated as experimental products of the Centre's forecast should be consistent with the computation of the fluxes described above. In principle (1) and (2) form a system of equations which can be solved for ∇ and θ at any height, given the surface fluxes P_M and P_H. However the analytical form of these equations make the solution of this system rather difficult. Hence we do an approximate computation where we first calculate the equivalent roughness length z_o' which would produce the same surface fluxes assuming the logarithmic profile, i.e. z_o' is such that:

$$[\, k \,/\, \ln(h/z_o')\,]^2 = [\, k \,/\, \ln(h/z_o)\,]^2 \cdot F(h/z_o, Ri) \qquad (3)$$

Then we use the logarithmic profiles (i.e. Equ.2 with F=G=1) with this equivalent roughness length to compute V at 2 and 10 m and θ at 2 m. A similar interpolation of the humidity is used to compute the dew-point temperature at 2 m.

It should be noted that, so far, the diurnal variation of the solar radiation has not been included in the operational model: we use, as solar input, the average over 24 hours. This means that one should compare the near-surface variables produced by the model with the averaged observed values and not instantaneous ones. In addition, the absence of diurnal cycle is likely to produce too small a depression of the dew-point temperature.

3. MOIST PROCESSES

We distinguish two kinds of clouds in the forecast model: stratiform and convective.

The treatment of stratiform clouds is quite simple. It is assumed that, whenever the total humidity of a grid point becomes greater than its saturation value, the excess moisture condenses and the corresponding latent heat is released. This excess moisture, however, is not necessarily removed as rain immediately. It only precipitates if either the top level of the cloud is cold enough (below -12 C) or the total liquid water content of the column is large enough (greater than 2 mm). The first criterion takes into account the greater efficiency of ice nuclei at low temperature. The second condition crudely simulates the fact that in a deep cloud the droplet distribution has a wider spectrum than in a thin cloud and the coalescence of droplets into rain drops is more rapid. Finally, as the rain falls, it can re-evaporate in the drier layers below the cloud.

The main weakness of this scheme is the assumption that condensation can occur only when the grid point is entirely saturated, even though it is fairly obvious that stratiform clouds can exist which do not entirely fill a volume nearly 200 km on the side and up to 100 mb thick. In order to overcome this difficulty one would need some additional information such as the mixing ratio of liquid water in the clouds and the variance of humidity in the volume. A drawback of the present scheme is that we only have one prognostic variable for moisture in the model: the total amount of water. Hence we cannot advect separately the water vapour and the liquid water and, at each time step, the liquid water is diagnosed as the amount which is supersaturated. We have preferred to choose 100% relative humidity as the critical value rather than some arbitrary lower value. In a future model we shall have a prognostic variable for the amount of liquid water and we may also be able to relax this 100% relative humidity criterion.

Our convective precipitation scheme follows closely the method proposed by Kuo (1965, 1974). A convective cloud exists when there is a net convergence of moisture into a conditionally unstable layer. The amount of cloud air is computed as the ratio of the latent heat contained in the converging water vapor to the excess moist static energy of the cloud. Part of the moisture contained in the cloud is then mixed with the environment, while the rest rains out, releasing its latent heat. This fraction is determined by the relative humidity of the environment. Again, some of the rain can re-evaporate below the cloud.

One should be aware that the division between stratiform and convective precipitation is somewhat arbitrary and model-dependent. As an illustration of this statement we show in figure 3 two forecasts done with the limited area version of the Centre's model. One was done with the operational model. In the other forecast the Kuo convection scheme was replaced by a method proposed by Arakawa and Schubert (1974). It can be seen that, although the

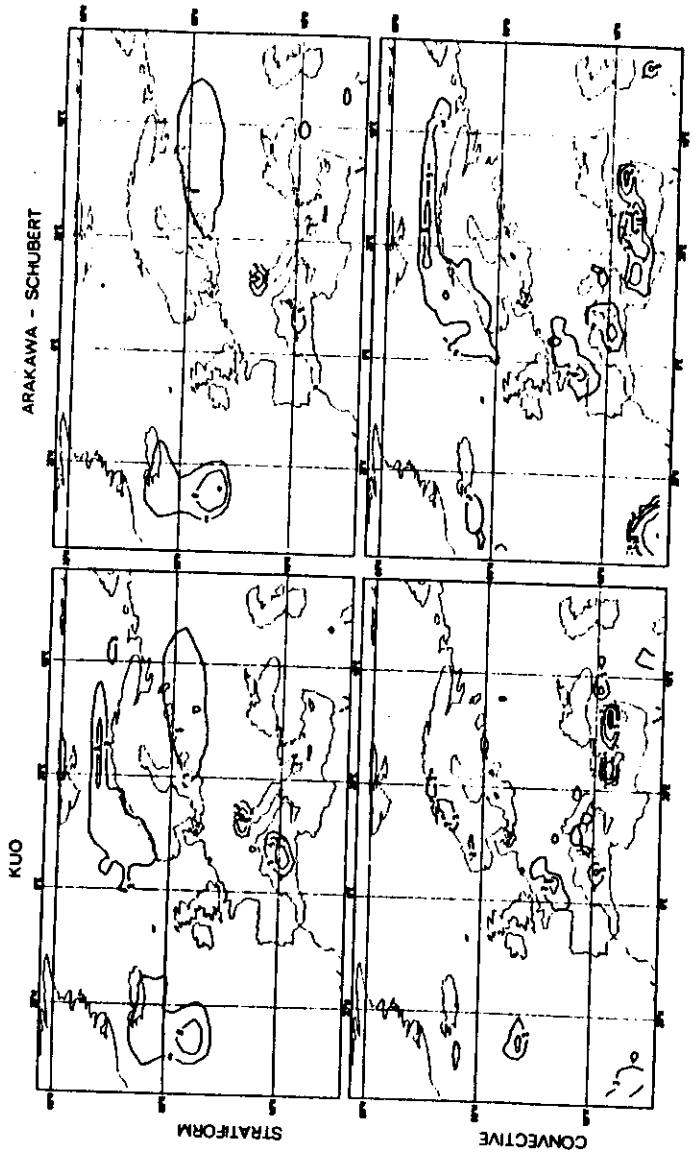

Fig. 3 Comparison of two 24-hour precipitation forecasts

total precipitation is nearly the same in the two forecasts, the partition between stratiform and convective precipitation is very different in the polar region. Another thing which might be worth mentioning is that, at the moment, no distinction is made between snow and rain within the cloud. It is only when the precipitation reaches the ground that it is assumed to be snow if the surface temperature is below 0 C, or rain otherwise. This means that there is a slight energetic inconsistency between the treatment of the clouds and that of the surface processes where we do take into account the heat necessary to melt the snow. This inconsistency will be removed in the future.

4. RADIATION

One can look at the role of radiation in the atmosphere from two different points of view. Globally, radiation provides the primary source of energy for the atmosphere and maintains the thermal gradient between the equator and the poles. Locally, radiation has a large effect on the weather by driving the boundary layer processes and affecting the development of clouds. The importance of the cloud-radiation interactions is obvious for the local weather, but it is no less important for the global heat balance.

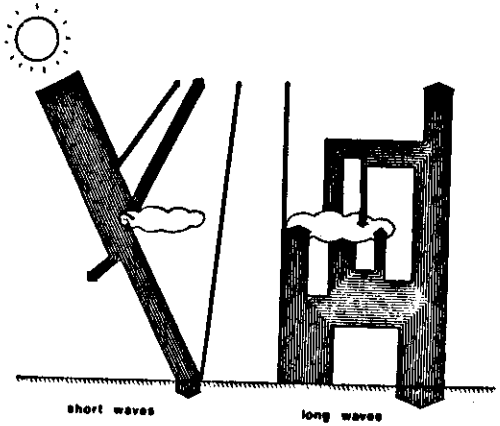

Fig. 4 Qualitative description of the radiative fluxes in the earth/atmosphere system

The diagram of figure 4 illustrates this statement. It describes, in a very schematic way, what happens to the radiative fluxes in the atmosphere. The left side of the figure represents the short wave fluxes, while the right side shows the long wave fluxes. I have not put any numbers on the figure because some of the components are still rather uncertain, but the thickness of the arrows is approximately proportional to the magnitude of the fluxes. The short wave diagram is fairly straightforward, showing that, although little of the sun light is absorbed by the clouds, about one third of the incident solar radiation is reflected by them. The long wave fluxes are a bit more difficult to represent in such a diagram because a lot of absorption and re-emission takes place within the atmosphere, but since the clouds are nearly black bodies in the infra-red, they are clearly important in the transfer of long wave radiation.

In view of the importance of cloud-radiation interactions in both long and short term processes, we have placed a high emphasis on the treatment of the clouds in the radiation scheme. Hence the grey processes are computed first: absorption and scattering by clouds and aerosols, and Rayleigh scattering by the air molecules. In this calculation clouds are allowed to occur in any layer of the model and multiple scattering is taken into account. Then the absorption and emission by the gases (CO_2, H_2O, and O_3) modifies the fluxes resulting from the first part of the computation.

The main problem for the parameterization is to determine the cloudiness of each layer of the model. We cannot, unfortunately, use the information from the parameterization of the moist processes since, with the 100% relative humidity criterion for condensation, we would never have partial cloudiness. Also in its present implementation the Kuo convection scheme does not give us any information on the lateral extent of the cumulus clouds.

We have then used statistics of Pham and Rousseau (1976) on the relationship between relative humidity and the frequency of moist adiabatic lapse rate to evaluate a regression curve between cloudiness and relative humidity. This curve is shown on figure 5 for the 500 mb level. The critical relative humidity below which no clouds are assumed to exist is a inverse function of height. In each layer of the model a fraction of the area corresponding to the curve in figure 5 is assumed to be entirely filled with clouds, and the radiative fluxes are computed separately in the cloudy and clear parts. When clouds exist in two adjacent layers, maximum overlap of the cloudy parts is assumed.

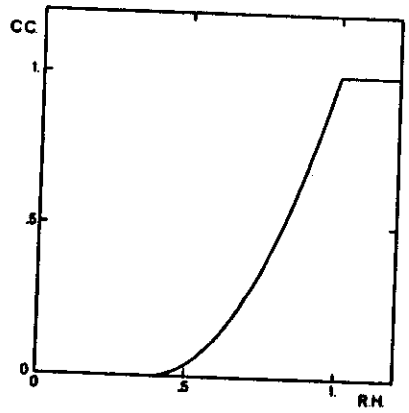

Fig. 5 Assumed relationship between cloud cover and relative humidity at $p/p_s = 0.6$.

It is evident that such a parameterisation is very crude, and likely to be poor in the regions which have either tall cumuli penetrating into dry layers, or thin clouds which would not entirely fill a whole layer of the model. The latter problem is particularly bad in the case of thin stratus clouds developing at the top of the boundary layer. Radiation is important in the development of these clouds, with strong cooling at the top and warming within the cloud which destabilises the cloud layer. In the model, however, with a relatively coarse vertical resolution and our assumption that the cloud occupies the whole model layer, the effect of radiation tends to destabilise the whole boundary layer and produce a wrong feed-back involving vertical diffusion and condensation. In order to avoid an exaggerated precipitation in this situation we have been forced to suppress the clouds at the top of an unstable boundary layer, as far as the radiation scheme is concerned.

Once we introduce a prognostic variable for the liquid water content we hope to be able to connect in a more consistent fashion the cloudiness in the radiation scheme and the liquid water determined by the moist processes. At any rate this cloudiness parameter is a quantity which can be directly compared to observations. This is why we routinely produce pseudo-satellite pictures which are simply this radiation cloudiness, integrated over all the levels, and plotted as various shades of grey. An example is given in figure 6, compared with the actual satellite photograph.

5. GROUND PROCESSES

The model has prognostic equations for the surface temperature and moisture. At the time of writing, the method of computing these variables is about to be modified, and I shall describe the new scheme. It is designed so that we can switch on the diurnal cycle which, as already mentioned, is now suppressed. The scheme is a straightforward simulation of the diffusion equation in the ground, using a finite difference scheme with three layers. The top layer is thin enough to react to the daily cycle. The second layer responds to changes with time scales of about a month. Finally, a climate value is imposed in the bottom layer. The boundary condition at the top is the net flux at the surface: radiative, sensible and latent heat fluxes for the temperature; precipitation and evaporation for the moisture.

Nearly a year ago, a bulk parameterization scheme was introduced, following the ideas of Deardorff (1978). Various problems with our implementation of this scheme have delayed a subsequent introduction of the diurnal cycle. We hope that these difficulties will be avoided with this new scheme so that we can turn on the diurnal cycle soon.

Another element of the parameterization which is important for the radiation is the treatment of the snow, since there is a strong feed-back between the

ECMWF 24 hr forecast for 19-7-81

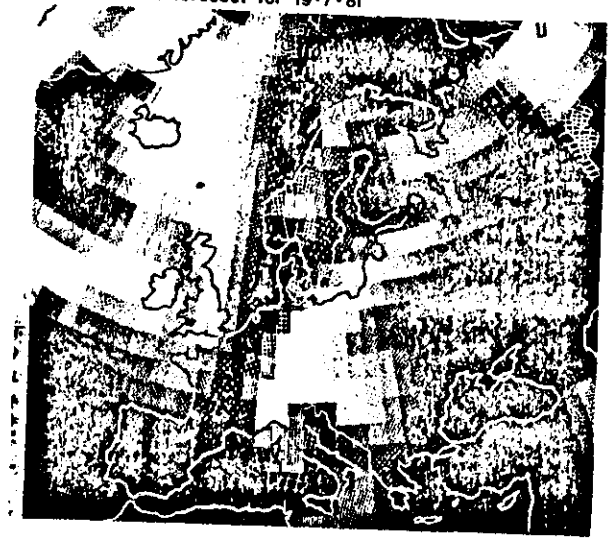

NOAA-6 satellite photograph (visible)

Fig. 6 An example of a 24-hour cloudiness forecast, with the corresponding satellite photograph

albedo and the ground temperature in the presence of snow. Snow is assumed to have an albedo of 0.8. However, in order to avoid shocks which might produce noise in the forecast, we assumed that the albedo changes smoothly between the value of the bare ground and that of the snow, depending of the snow cover which is taken as a monotonic function of snow depth. The albedo value of 0.8 is reached when the snow depth is about 1 m.

There are a number of weaknesses in the treatment of the snow in the operational model. I have already mentioned that precipitation is assumed to be snow only when the ground temperature is below freezing. Another problem, which is due to the fact the we do not carry information about vegetation in the model, is that we do not take into consideration the fact that forest can have a relatively low albedo, even with deep snow, if it is windy. The change of albedo with the age of the snow is not considered either. Finally, and probably most important, is the fact that we do not change the heat capacity and conductivity of the ground when snow is present. This results in frequent overestimation of the snow covered ground temperature and too rapid melting of the snow. We hope to correct this latter problem some time in the near future.

6. CONCLUSION

I hope that this quick overview of the parameterisation schemes of our forecast model has given the reader an idea of the methods we use. It is evident that all the schemes are fairly simple, even though they nonetheless represent the current state of the art in large scale model parameterization. One reason for this simplicity is the need for fast computation. In the present operational model the parameterisation takes up about 50% of the whole computing time. We would not want this figure to increase too much with more sophisticated methods. Already we are forced to perform the radiation calculation only twice per forecast day because it would be prohibitively expensive to do it more often in its present form.

In addition to the need for fast computation, we also prefer to keep our schemes simple, (with few arbitrary parameters) in order to understand their behaviour more easily; but at the same time we try to include in the schemes all the significant interactions between the various processes, in order to simulate as well as possible the effect of all the feed-back loops. In future development, we shall try first to remove some of the inconsistencies which still exist, such as the different definition of cloudiness in the condensation and radiation, problems with the snow, and the absence of diurnal cycle.

REFERENCES

Arakawa,A., Schubert,W.H., 1974: Interaction of a cumulus cloud ensemble with the large-scale environment, part I. J.Atmos.Sci.,31,674-701.

Deardorff,J.W., 1978: Efficient prediction of ground surface temperature and moisture, with inclusion of a layer of vegetation. J.Geophys.Res.,83, 1889-1903.

Geleyn,J-F., Hollingsworth,A., 1979: An economical analytical method for the computation of the interaction between scattering and line absorption of radiation. Beitr.Phys.Atmos.,52,1-16.

Kuo,H.L., 1965: On formation and intensification of tropical cyclones through latent heat release by cumulus convection. J.Atmos.Sci.,22,40-63.

Kuo,H.L., 1974: Further studies of the parameterization of the influence of cumulus convection on large-scale flow. J.Atmos.Sci.,31,1232-1240.

Louis,J-F., 1979: A parametric model of the vertical eddy fluxes in the atmosphere. Boundary-Layer Meteor.,17,187-202.